The selective dynamical downscaling method for extreme-wind atlases

Larsén, Xiaoli Guo; Badger, Jake; Hahmann, Andrea N.; Mortensen, Niels Gylling

Published in:
Wind Energy

Link to article, DOI:
10.1002/we.1544

Publication date:
2012

Document Version
Early version, also known as pre-print

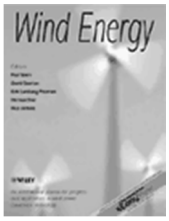

The selective dynamical downscaling method for extreme wind atlases

Journal:	*Wind Energy*
Manuscript ID:	WE-12-0042.R2
Wiley - Manuscript type:	Research Article
Date Submitted by the Author:	n/a
Complete List of Authors:	Larsén, Xiaoli; Technical University of Denmark, Department of Wind Energy Badger, Jake; Technical University of Denmark, Department of Wind Energy Hahmann, Andrea; Technical University of Denmark, Department of Wind Energy Mortensen, Niels; Technical University of Denmark, Department of Wind Energy
Keywords:	Extreme wind atlas, WRF, selective dynamical downscaling, post-processing, storms

WIND ENERGY

Wind Energ. 2012; **00**:1–25

DOI: 10.1002/we

RESEARCH ARTICLE

The selective dynamical downscaling method for extreme wind atlases

Xiaoli Guo Larsén, Jake Badger, Andrea N. Hahmann and Niels G. Mortensen

Department of Wind Energy, Risø Campus, Technical University of Denmark, 4000 Roskilde, Denmark

ABSTRACT

A selective dynamical downscaling method is developed to obtain extreme wind atlases for large areas. The method is general, efficient and flexible. The method consists of three steps: (i) identifying storms episodes for a particular area, (ii) downscaling of the storms using mesoscale modeling and (iii) post-processing. The post-processing generalizes the winds from the mesoscale modeling to standard conditions, i.e. 10 m height over a homogeneous surface with roughness length of 5 cm. The generalized winds are then used to calculate the 50-year wind using the Annual Maximum Method for each mesoscale grid point. The generalization of the mesoscale winds through the post-processing provides a framework for data validation and for applying further the mesoscale extreme winds at specific places using microscale modeling. The results are compared to measurements from two areas with different types of extreme wind climates and the results are promising. Copyright © 2012 John Wiley & Sons, Ltd.

KEYWORDS

Extreme wind atlas, WRF, selective dynamical downscaling, post-processing, storms

Correspondence

Xiaoli G. Larsén, xgal@dtu.dk

Received . . .

Prepared using weauth.cls [Version: 2010/06/17 v1.00] JohnWiley&Sons

1. INTRODUCTION

With the rapid development of wind energy, there is an increasingly urgent need for accurate estimation of the design wind speed for wind turbines in order to make sure that winds will not exceed the turbine's design specification or to avoid turbine design being unrealistically over-specified. This design wind speed, also called the extreme wind, is usually defined as the 50-year wind. In the current European Load Code [1], it is referred to as the 10 min averaged wind, which, on average, occurs with a return period of 50 years.

The estimation of the 50-year wind often assumes that the extreme wind events satisfy a certain distribution, e.g. the Gumbel [2], the Reverse Weibull or the Frechet [3] distribution, and the uncertainty of the estimation decreases with increasing sample size. This has always been the most difficult issue because there lacks long term measurements of reliable quality. In most industrial applications, there are often only five years, or less, of data. In many commercial projects, in order to increase the sample size, often a lower wind speed threshold is used while using the Peak-over-Threshold method or a shorter basis period is used when using the Periodic Maximum Method (e.g. [4]). A possible consequence of the use of these techniques is a very high uncertainty [4] because the preconditions for applying these statistical models are often violated, e.g. the requirement of independent samples and the requirement of the samples being from the same type of underlying meteorological mechanism. At the same time, other studies use mathematical approaches (e.g. Monte Carlo method) to simulate time series of hundreds or thousands of years (e.g. [5, 6]). As it is questionable that the time series from the mathematical simulations carries the natural variability observed in the extreme wind climate, many make use of the physical models instead, such as numerical weather prediction (NWP) models to obtain wind climate many years back.

Atmospheric reanalysis projects, such as those carried out by NCEP/NCAR (National Centers for Environmental Prediction/National Center for Atmospheric Research [7]) and ECMWF (European Center for Medium range Weather Forecasting), use a large volume of measurements available and assimilate them into NWP models, and thus provide us with decades long, physically based, data sets over the globe. Frank et al. [8] and Larsén et al. [9] investigated the applicability of such reanalysis data for extreme wind estimation. Because of the coarse resolution of the data ($\sim$ 200 km), the authors do not use the reanalysis winds directly but downscale the geostrophic wind calculated from the pressure and temperature fields through a microscale model. This is analogous to the concept used in the widely used software for wind energy WAsP and WAsP Engineering (WEng) that relates the geostrophic wind to the "surface wind" through the geostrophic drag law ([10]). Here this "surface wind" is an intermediate, but central, parameter. It satisfies the so-called standard conditions: 10 min value over a homogeneous surface with a certain surface roughness length (e.g. 5 cm) at a

certain reference height (often hub height or 10 m above ground). This surface wind is often called the "standard wind" (e.g. [11]) or "generalized wind" ([12]) and it serves as the background reference for the microscale model in WAsP and WEng where the effects of the site specific topography and roughness are added and the local winds are eventually simulated. The approach of using measurements of pressure and temperature was first suggested by [13] and later carried out by [14, 15]. Compared to the long term record of wind speed, those for pressure and temperature are relatively easier to access. The reanalysis data make the application of this approach possible in many places over the globe. One big concern of this approach, which uses the microscale model directly from the global reanalysis data, is that variability added by mesoscale phenomena is ignored. As a result, it works reasonably well in places where the extreme winds are predominately due to synoptic weather phenomena, but in places where the extreme winds are predominately due to mesoscale mechanisms, the extreme wind estimation has large uncertainty, as shown by comparison with measurements ([9]).

To resolve better the variability resulting from mesoscale phenomena, many investigators have used outputs from various Regional Climate Models (RCMs). However, the RCM run-based studies have focused on general statistics of storms and strong winds (e.g. [16, 17]), or modeling of a single storm (e.g. [18]), rather than the extreme winds for wind energy site applications. Using output of a horizontal grid spacing ranging from 10 km to 50 km, [19] demonstrated that, due to the smoothing effect of mesoscale models, the zero- and second-order moments in the wind speed spectra are severely underestimated, which leads to significantly underestimated extreme winds. This reflects the fact that such RCMs do not completely resolve the mesoscale variability that is essential for extreme wind estimation. Another problem with some of the RCMs is that, after the model initiation, the models are only constrained by the boundary conditions, which sometimes results in storms that do not follow the same track as in the large scale data ([20]). One might argue that the simulations, for say 50 years, are long enough and may have the extreme wind climate captured, and accurate simulation of actual individual storms is not crucial. However, there is still a lack of evidence showing success for such a climate simulation. In other words, it is a problem that the storms that are essential for extreme wind are not well resolved in RCMs. In [21, 22, 23], the 50-year wind was calculated directly from the RCMs output, but the fact that these numbers are more suitable for studies of climate change and trend means they should not be used directly as site conditions of wind farms.

To address these issues, instead of making a continuous simulation for decades, we put the focus on simulating individual storms that are directly relevant for the extreme wind estimation by using the mesoscale Weather Research and Forecasting (WRF) model (Section 2.2 and 2.3). Because we are interested in the variability caused by mesoscale phenomena, the standard winds that link the large- and micro-scale variability should not be calculated from the pressure

gradient as done in [9] because the ageostropic part of the flow should also be considered. The post-processing procedure (Section 2.4) is therefore a core element of this method; it calculates the speed-up effects of orography, and roughness change in the upwind fetches, and corrects the winds from the mesoscale model output to the standard condition. Thus, it not only provides an opportunity for reasonable data validation but is also necessary in order to prepare the winds from the mesoscale modeling for using the microscale modeling, here using WEng.

In the current study, the selective dynamical downscaling method is applied to estimate extreme winds in two areas; one is over Denmark and surrounding waters where the meteorological mechanism of the extreme wind is through synoptic low pressure systems and the other is over the Gulf of Suez, where the channeling of the flow due to topography contributes significantly to the generation of the extreme winds ([24]). The details of the method are given in section 2. The results, including the strong wind episodes statistics from both measurements and simulations, as well as the extreme winds themselves, are presented in Section 4. Discussions and Conclusions follow in Sections 5 and 6.

2. THE SELECTIVE DYNAMICAL DOWNSCALING MODELING METHOD

The word "selective" refers to the selection of the annual strongest wind episodes. A statistical method, the Annual Maximum Method (AMM), is used here for calculating the 50-year wind (Section 2.1). There are three main steps in applying the method which are explained separately in Section 2.2 to 2.4.

2.1. The Annual Maximum Method

The distributions of the measured annual maximum wind speeds at all sites were examined and it was found that a generalized extreme wind distribution with a shape factor of zero, namely the Gumbel distribution, can best describe the data. The same is true for the simulated annual maximum winds at the corresponding model grid points closest to the sites, see Figure 1 for an example. It is possible that in some areas where the extreme wind climate is more complicated, e.g., with multiple dynamics contributing to the extremes and with each having its own distribution, the shape factor is a considerable positive value, and this will result in a significantly larger U_T at a large return period T. It has been argued in the literature that the Gumbel distribution is not realistic at very large T due to its unbounded high values while it is more realistic with the so-called Reverse Weibull distribution with a negative shape factor because it provides a limiting return winds ([25, 3]). However, studies have shown that the difference in U_T is minor for T at about 50 years by using Gumbel

Wind Energ. 2012; **00**:1–25

JohnWiley&ons

DOI: 10.1002/we

Prepared using weauth.cls

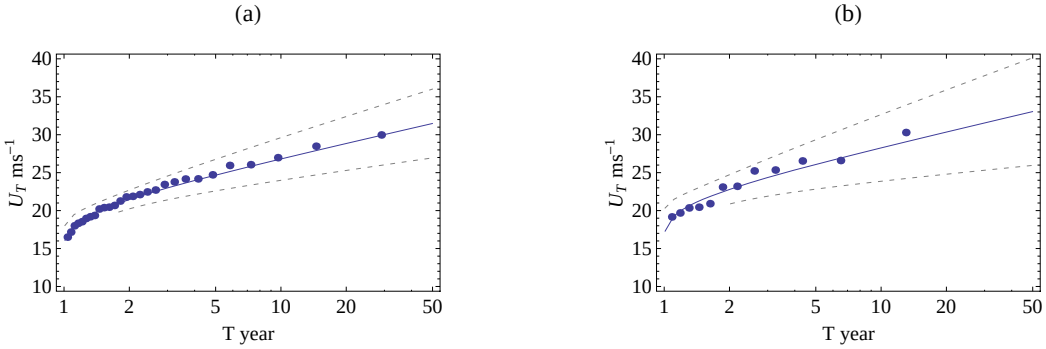

Figure 1. An example of the annual maximum wind (in dots) distribution at Tystofte, (a) measurements at 39 m (28 years) (b) WRF simulated winds at 52 m (12 years) at the grid point closest to the site. For both, the solid curve is the Gumbel distribution and the dashed curves are the 95% confidence interval.

or Reverse Weibull distributions (e.g. [25]). The Gumbel distribution is therefore used here for the annual maximum wind to obtain U_T and this is the Annual Maximum Method (AMM).

A more detailed derivation of AMM can be found in [26]. Briefly, the annual wind maxima from n years are first sorted in ascending order as U_i^{max}, where $i = 1, ..., n$. Then, the Gumbel extreme wind distribution is used to fit the set of annual wind maxima ([2, 9]) and eventually the T-year wind speed, U_T, is obtained from

$$U_T = \alpha^{-1} \ln T + \beta, \tag{1}$$

where the coefficients α and β are obtained through the probability-weighted moment procedure

$$\alpha = \frac{\ln 2}{2b_1 - \overline{U^{max}}}, \ \beta = \overline{U^{max}} - \frac{\gamma_E}{\alpha}, \tag{2}$$

where $\gamma_E \approx 0.577216$ is the Euler constant, $\overline{U^{max}}$ is the mean of U_i^{max} and b_1 is calculated from

$$b_1 = \frac{1}{n} \sum_{i=1}^{n} \frac{i-1}{n-1} U_i^{max}. \tag{3}$$

According to [26] and [27], the probability weighted moment procedure gives little bias and variance on the parameter estimates and is very efficient for small size samples.

DOI: 10.1002/we

Mann et al. [4] gave the estimation of uncertainty of U_T, which is calculated from uncertainties on α and β:

$$\sigma(U_T) = \frac{\pi}{\alpha}\sqrt{\frac{1 + 1.14k_T + 1.10k_T^2}{6n}} \tag{4}$$

with

$$k_T = -\frac{\sqrt{6}}{\pi}\left[\ln\ln\left(\frac{T}{T-1}\right) + \gamma_E\right] \tag{5}$$

The uncertainty due to the fitting is estimated as the 95% confidence interval here and it is obtained by $1.96 \cdot \sigma(U_T)$, where $\sigma(U_T)$ decreases with increasing sample number n.

2.2. Identifying the storms

We use the NCEP/NCAR reanalysis (NRA) data to identify the storm episodes in the climate record. The NRA data are 6 hourly with a horizontal grid spacing of about 200 km. The period 1999 - 2010 is chosen instead of the entire NRA since 1948, because the NCEP Final Analysis (FNL) data are used as the boundary forcing of the WRF modeling and they are only available from 1999. As in the NRA data, the FNL data are also 6 hourly, but with a horizontal spacing of 1°. We use the relatively short FNL data record for obtaining the extreme wind atlas rather than the long duration NRA data because individual storms are significantly better simulated using the FNL data than using the NRA data (see details in Section 2.3).

Two parameters are used for the storm identification: the wind speed at 10 m and the geostrophic wind at sea level, G. The algorithms for computing G using the reanalysis pressure and temperature can be found in [9]. For Denmark, there are 5×4 NRA grid points in the chosen area (Figure 2a), and for the Gulf of Suez, there are 3×3 grid points in the area (Figure 2b). For each grid point, the dates when the yearly strongest geostrophic wind and the yearly strongest 10 m winds occur, which are not always the same, are identified. For Denmark, this results in 20 (grid point numbers)$\times$12 (years) $\times$2 (G; 10 m wind speed) time stamps. Some of the time stamps belong to the same storm. Altogether, for the period 1999 to 2010, we collect 59 storm episodes for the region in Figure 2a (Denmark) and 57 storm episodes for the region in Figure 2b (Gulf of Suez). The number of storms for the much larger domain over Denmark is similar to the smaller domain for the Gulf of Suez, reflecting that the scale of typical extreme wind system is much larger in Denmark than in the Gulf of Suez. Note, the larger area we define, the more NRA grid points are obtained, the more storms are likely to contribute to the extreme wind atlas.

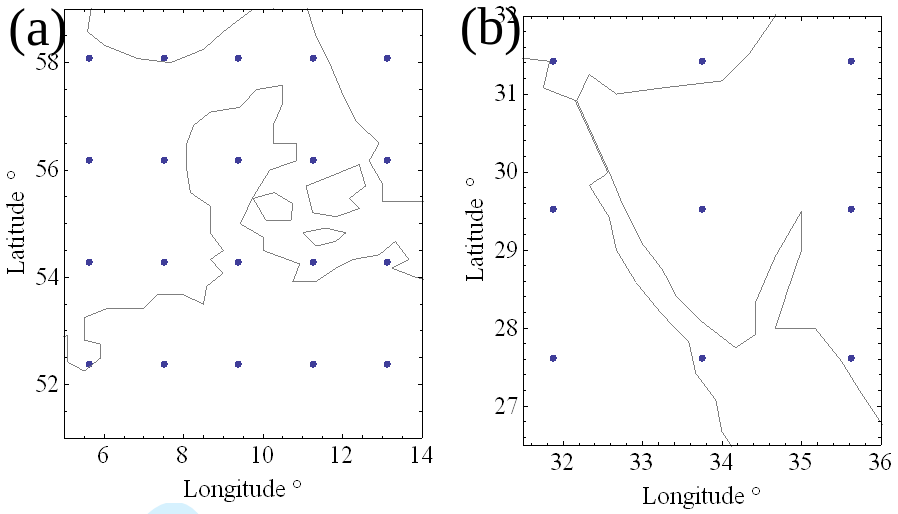

Figure 2. Region of interest and grid points (dots) of the NCEP/NCAR reanalysis data for storm identification, (a) Denmark; (b) Gulf of Suez. See the locations of the two domains in larger maps in Fig. 3.

2.3. Simulation of the storm episodes

The Advanced Research WRF (ARW) core version 3.1 was used for the mesoscale modeling. Both NRA and FNL data have been tested as the initial and lateral boundary forcing. It was found through a number of case studies that, compared to the NRA data, the spin-up time when using the FNL data is only one to two hours while when using the NRA data it can be six hours or more. It was also found that when the storms are simulated using FNL as forcing, the simulations better predict the track and intensity compared to those using NRA. Because of its higher spatial horizontal resolution, the FNL data has better resolved storm structures already in the initial conditions. The FNL data are therefore used as the initial and lateral conditions for the simulation of all storms. Together with the FNL data, the half degree NCEP Reynolds Optimally interpolated sea surface temperature data set is used. The sea surface temperature is however only available from 2001.

For a particular storm, the start time of the simulation is set at 24 hours before of the first NRA time stamp and the end time of the simulation is set at 24 hours after the last NRA time stamp. For instance, for the storm in November 2010, two storm stamps were identified in the NRA data, 2010-11-11 06:00 and 2010-11-11 12:00, the start of the simulation is thus set to be 2010-11-10 06:00 and the end is set to be 2010-11-12 12:00. Because individual extreme wind events, both in Denmark and Gulf of Suez, do not usually last more than three days, the simulation length is thus limited to $2-3$ days.

Different physics options have been tested through a number of case studies and the final choices include Lin et al. microphysics scheme, Kain-Fritsch cumulus parameterization, 6th order numerical diffusion with factors 0.06, 0.08 and 0.1 for the three domains, and positive definite advection of moisture and scalars. Through case studies, we concluded that

DOI: 10.1002/we

the differences due to using different schemes are minor compared to that caused by using NRA data, by the uncertainties related to the post-processing procedure, or by the statistic method for the return wind. The selection of Yonsei University Planetary Boundary Layer (YSU PBL) scheme is based on two facts, the findings in [28], where YSU PBL scheme performs well in simulating typhoon events and the findings in [29], where YSU PBL outperforms six other PBL schemes for neutral conditions, which are often the storm conditions due to the strong winds. The hurricane option for surface roughness is chosen, i.e. the drag coefficient increases with wind speed when wind speed at 10 m is smaller than 32 ms^{-1} and starts to decrease at greater wind speed at 10 m. Further details of these parameterizations can be found in [30].

The WRF configuration used has three nested domains of different size. Because of the different characteristics of the extreme wind events in the two regions, we set the horizontal grid spacing to 45 - 15 - 5 km for Denmark (Figure 3a) and to 27 - 9 - 3 km (i.e. finer) for the Gulf of Suez (Figure 3b) for domain I, II and III, respectively. We denote the horizontal grid spacing in domain III as Δx. There are 37 vertical levels in all domains. One-way nesting is used. The time step for domain I is 4 minutes for Denmark and 2 minutes for the Gulf of Suez. The output is recorded every 10 minutes. When all storms are simulated, at each grid point in domain III, 12 annual maximum wind speeds with corresponding wind directions are determined.

2.4. The post-processing procedure

The post-processing procedure is a must for quantitative data validation. Simulated data and measurements can only be compared "qualitatively" without post-processing, because the mesoscale winds are spatially averaged values representative for the area of the grid box size. The average topography and roughness over the grid box is often very different from the site where measurements were taken, especially in complex terrain, e.g. in coastal and mountain areas. It has always been a challenge to verify a modeled field with measurements. A thorough review of existing verification techniques can be found in [31, 32]. However, here we look for a technique that not only provides some general statistics of the modeled winds in comparison with measurements, but a wind magnitude and direction that can further be used for a siting a wind farm. Such a technique for linking mesoscale and microscale modeling has recently been initiated by [12] and it is not included in the reviews of [31, 32]. The post-processing generalization procedure converts both the measured and modeled winds to a standard condition, over a homogeneous surface with a reference roughness length (e.g. 5 cm) at a reference height (e.g. 10 m). To some extent, the concept here agrees with the technique described in [33] where both simulated and modeled precipitation were upscaled to a coarser resolution before the validation. However, our approach uses a flow model to transform the wind between different topography and surface roughness, thus keeping the

JohnWiley&ons DOI: 10.1002/we

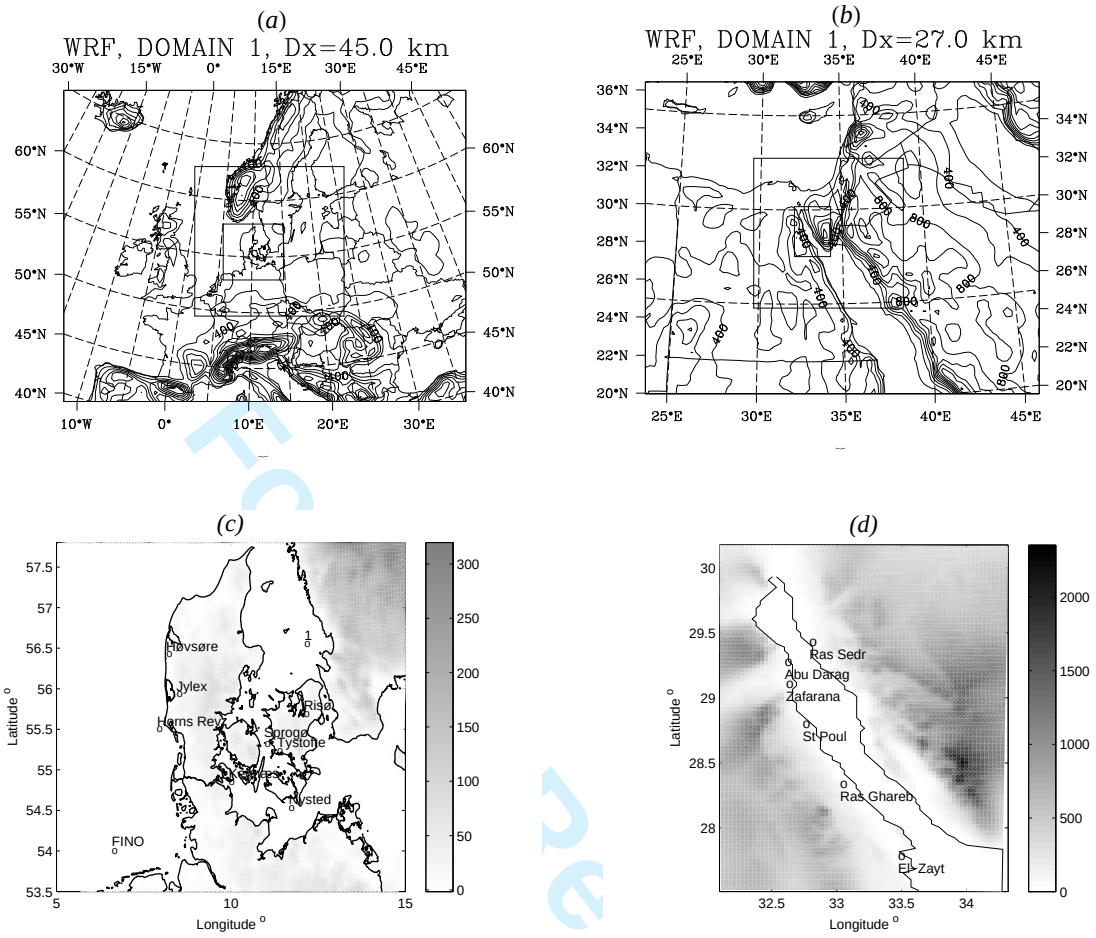

Figure 3. Three model domains of the WRF modeling shown as the topography contours for Denmark (a) and Gulf of Suez (b), respectively. The measurements sites are shown on the elevation (m) maps for Denmark (c) and for the Gulf of Suez (d), being in the innermost model domains as in (a) and (b). Refer to Table II for details of the sites.

wind variability consistent through the physical description in the mesoscale model condition, the standard condition and the turbine site condition. This can not be done using the averaging approach in [33]. The generalization also provides a framework for comparing results from different methodologies and across regions once these values are all converted to the same surface conditions ([34, 1]).

Briefly, to introduce the generalization process, the speed-up effects due to local orography (e.g. speed-up at hills) and roughness change in the upstream sectors are first calculated and they are represented as the coefficients s_o and s_r, respectively. An effective roughness length is also calculated for each sector, as the area-averaged roughness in the upstream fetch, and denoted as z_0. The details of the models used for calculating these coefficients can be found in [35, 36]. In the following, we show how the parameters are used. Firstly, to remove the speed-up effects of orography and

DOI: 10.1002/we

roughness change for each sector, using the coefficients s_o and s_r, the flat homogeneous terrain wind speed u_z at a height of z and uniform roughness z_0 is obtained through:

$$u_z = \frac{u_{0,z}}{(1+s_o)(1+s_r)}, \tag{6}$$

where $u_{0,z}$ is the wind speed at height z. The corresponding surface friction velocity, u_*, can then be calculated with u_z and z_0, for each sector through the surface logarithmic law:

$$u_* = \frac{\kappa u_z}{\ln(z/z_0)}, \tag{7}$$

where $\kappa = 0.4$ is the von Kármán constant. The geostrophic wind, G, is calculated from u_* through the geostrophic drag law (e.g. [10]):

$$G = \frac{u_*}{\kappa}\sqrt{\left(\ln\frac{u_*}{fz_0} - A\right)^2 + B^2}, \tag{8}$$

where f is the Coriolis parameter, and $A = 1.8$ and $B = 4.5$ are dimensionless parameters according to [37]. Neutral stability condition is assumed, which is usually a reasonable assumption when the winds are very strong. The fundamental principle of this process is that G remains the same before and after the generalization. Under the same G but a new roughness length for the standard condition, here $z_{0,r} = 0.05$ m, a new friction velocity, $u_{*,r}$, is obtained through Eq. (8). Using this new set of $u_{*,r}$ and $z_{0,r}$ and Eq. (7), we obtain the standard wind u_{st}.

The generalization is applied to both the measurements (for validation) and for the modeled winds. For measurements, the winds are generalized using the standard procedure embedded in WEng through the Linear Computational model LINCOM. For the modeled winds, LINCOM calculates, for all mesoscale model grid points, the perturbation to the wind speed given by orography and roughness change for a number of sectors; here 12 sectors are used. These perturbations are expressed as generalization factors, which are height and sector dependent. The effective roughness length and generalization factors form a look-up table for each mesoscale model grid point and each sector. For each of the storm episodes, the application of the generalization procedure is then done following the procedure described above, which are put into four steps as given in Table I.

For grid points over water, there is no dynamical coupling of the atmospheric modeling to the underlying water waves mechanisms. The water roughness length in the WRF model is described with two terms $z_0 = z_{0,ch} + z_{0,s}$, where $z_{0,ch}$ is from the Charnock formulation [38] $z_{0,ch} = \alpha_{ch} u_*^2/g$, with the Charnock parameter $\alpha_{ch} = 0.0185$ and $z_{0,s}$ is set as a

Table I. Description of the generalization of the WRF winds.

Step	Equations	Action
1	Eq. (6)	Apply the generalization factors to the simulated wind to obtain a modified simulated wind
2	Eq. (7),(8)	Use the effective roughness length and the corrected simulated winds to obtain u_* and G
3	Eq. (8)	Use iteration for the new roughness length, here $z_{0,r} = 0.05$ m, to obtain new frictional velocity $u_{*,r}$
4	Eq. (7)	Obtain u_{st}, with $z_{0,r}$ and $u_{*,r}$ as input

constant of $1.59 \cdot 10^{-5}$ m, a typical value for smooth water surface. For our case, the smooth sea roughness is negligible. The Charnock formulation was derived for fully developed, wind generated waves over deep water. This is seldom the case over coastal waters, especially during storm conditions. We used measurements of turbulence fluxes and wind profiles from the offshore site Horns Rev and found that α_{ch} can be as large as 0.05 or greater during storms if we force the Charnock formulation to describe the roughness length. In doing so, the effects from shoaling of swell, the bathymetry, wave breaking and foaming are simplified. In the post-processing, α_{ch} is adjusted to 0.05. This gives a smooth transition of the generalized extreme winds from land to sea and visa versa (see Section 4). Using one single number for both the coastal areas and open water is still an oversimplification of the complex sea states. It is anticipated that there is larger uncertainty in the generalization in the very near coast areas (here approximately one to two grid points to the shore line).

3. MEASUREMENTS

The measurements are 10-min time series of wind speed and direction, air pressure and air temperature. The locations, measuring heights and period, for Denmark and the Gulf of Suez, can be found in Table II, as well as in Figure 3c and 3d, respectively.

These measurements build a network spanning the whole simulation period and across the whole area. It is thus not critical that some measurements of some parameters are missed at some sites. Not all the measured time series are long enough for an accurate estimation of the 50-year extreme winds and the measurement periods from the different sites do not necessarily overlap with the simulation period. We estimated the 50-year wind only when the length of the measurements is seven years or longer. The uncertainty related to the Gumbel fitting using a short time series could be significant and this should be considered when validating the results from the 12-year simulated extreme winds. Also, several sites, especially those from the Gulf of Suez, are located very near the coastal areas where it is most challenging for modeling and data validation.

Table II. Details of the measurements for the Denmark case (A) and Gulf of Suez case (B). (*) commercial site

	Station	Lat. (°N)	Lon. (°E)	Data period	Height (m)	Data coverage (%)
A	Sprogø	55.331	10.974	1977 - 1999	70	97.8
	Tystofte	55.24	11.33	1982 - 2010	39	96.7
	Kegnæs	54.856	9.936	1991 - 2006	23.4	99.5
	Jylex	55.942	8.449	1982 - 2004	24	96.4
	Risø	55.695	12.089	1996 - 2009	76.6	99.4
	Høvsøre	56.433	8.15	2004 - 2010	100	99.1
	Horns Rev	55.508	7.875	1999 - 2006	62	91.8
	Nysted	54.535	11.664	2004 - 2008	69	80.0
	FINO1	54.014	6.588	2004 - 2010	50	92.5
	c.s. (*)	56.561	12.105	2008 - 2010	60	99.2
B	Abu Darag	29.2803	32.5992	1991 - 2005	24.5	82
	Zafarana	29.1135	32.6108	1991 - 2005	24.5	79
	St. Paul	28.8035	32.7399	2000 - 2002	24.5, 47.5	58
	Ras Ghareb	28.3405	33.0269	2000 - 2005	24.5, 47.5	86
	Ras Sedr	29.4327	32.7904	2000 - 2005	24.5, 47.5	84
	Gulf of El-Zayt	27.79	33.4731	1994 - 2005	24.5	78

4. RESULTS AND VALIDATION

Two areas (Denmark and Gulf of Suez), representing extreme wind climates due to different meteorological mechanisms and scales, were selected for the production of the mesoscale extreme wind atlases. This is to test the feasibility of the methodology under various climates. For Denmark, the extreme wind events identified from measurements are fully captured by the NRA data for the overlapping period of measurements and modeling. For the Gulf of Suez, we expect that the topographical channeling contributes significantly to the extreme wind episodes. Therefore, there is a chance that these mesoscale events will not be represented in the coarse resolution NRA data. This is, however, not the case because the strongest channeling is linked to the large scale pressure distribution over the area. In total, about 80% of the storms identified in the measurements are captured by the NRA data for the overlapping period of measurements and NRA data. Some observed events were missed because their duration is shorter than 6 hours. The missed yearly strongest wind cases are filled in with the second or the third strongest wind event, which gives a difference between 0.1 and 2 ms^{-1} for the 10 min winds at the measuring height (24.5 m). The estimate of 80% should not be considered final, because at some sites the data coverage is poor (Table II). For such cases, the events identified in the measurements are likely not representative and the NRA data can serve as a compensation for the lack of measurements.

Model validation was done in the following manner: (i) qualitative comparison of the measured and simulated time series of a number of meteorological parameters (e.g. Figure 4); (ii) examination of the directional distribution of the 12 annual maximum wind events with the directional distribution of the measured five strongest wind events from each year (e.g. Figure 5); (iii) comparison of the power spectra of wind speed from modeling with those from measurements; (iv)

qualitative comparison of the measured and simulated actual 50-year wind at the measurement heights, U_{50} (Table III, column "no generalization"); (v) comparison of generalized 50-year wind, $U_{50,st}$, from measurements and modeling using post-processing (Table III, column "with generalization"). Quantitative and case sensitive statistics have been avoided for steps (i), (ii) and (iii) regarding the model and measurement difference, because the validation step (v) is the crucial one where uncertainties from each step in the methodology are added up. Quantitative calculations were however done for step (iv) to compare with the final results from step (v) and to show the effect of the post-processing procedure.

The WRF-derived time series of wind speed and direction, surface pressure and temperature during each individual storm were compared to available measurements at all sites. Figure 4 shows an example for the period of the 10th and 12th November 2010, at Tystofte. This example is arbitrarily chosen simply because there are measurements available for wind speed and direction, temperature and air pressure and it represents the typical variability of the measured and simulated variables during the simulation period. It is not expected that the simulated values here will be exactly the same as the measured ones, considering that variations in wind could be considerable within a grid box of 5×5 km^2. It is satisfactory that the wind pattern is well simulated, the storm peak strength is well captured and so is the lowest surface pressure.

The directional distribution of the strongest winds were examined in the same manner as the example shown in Figure 5. For Denmark, the modeling reproduces satisfactorily the dominating westerly strongest winds, as suggested in the measurements. For the Gulf of Suez (not shown), at the northernmost station on the east side of the channel, Ras Sedr, the extreme winds are from the south-east and the north-northwest sectors, suggesting the channeling effects causing it. At the three northern stations on the west side of the channel, Abu Darag, Zafarana and St Poul, the extreme winds are from three sectors, the north-northwest (channeling effect), the south-east (channeling effect) and the south-west directions (synoptic plus valley effect). At the two stations in the south, El Zayt and Ras Ghareb, measurements show that the extreme winds are from the north-northwest sector only (channeling effect). Good agreement between measurements and simulation is observed at all sites except for one site, Ras Ghareb (see Figure 3d for the location). At Ras Ghareb, the directional distribution of the annual maximum winds from the simulation at the closest grid point is similar to those at the three stations in the north (Abu Darag, Zafarana and St Poul) rather than one narrow sector around 330°, as suggested by the measurements. The winds at Ras Ghareb from the direction of 330° are a pure collection of the channeling winds and the corresponding WRF grid point has obviously included strong winds arising from other mechanisms. However, if we select a WRF grid point $2\Delta x$ closer to the channel, the agreement improves. This reflects the challenges in modeling in complex coastal areas.

As discussed in the Introduction, often, the outputs from RCM models do not reproduce the fine scale wind variability (see also Figure 4), having suffered from smoothing effects, and this is reflected as energy deficit in the power spectrum in the mesoscale range. As discussed in e.g. [39, 19], at the high frequency tail of the mesoscale range, instead of having a spectral slope of approximately $-5/3$ as climatological measurements have shown ([40]), the smoothing effect of modeling causes the energy to fall rapidly in smaller scales, with a steeper spectral slope of -3 or more. The power spectrum for each time series of the 10 min wind speed from each storm was calculated using a Fourier Transform, for both the measured and the modeled data. The wind conditions during the storms are rather non-stationary, which does not strictly satisfy the stationary conditions required for the applicability of Fourier Transform. However, it is important to understand how well the WRF spectra capture the high frequency variance, rather than the exact shape and energy level of these stormy winds. Figure 6 shows an example at Tystofte, Denmark, where the measurements are the longest and cover the entire period of the modeled winds. The spectra at all sites are calculated (not shown) and the results from different sites are similar. The spectra from the modeled wind time series, shown in Figure 6b, follow well the theoretical description although some of them are close to the slope of -2. Using the approach as described in [19], in comparison to a slope of $-5/3$, a slope of -2 gives an underestimation of the mean annual wind maximum $\overline{U^{max}}$ of less than 3%, which could be considered a small effect. On the other hand, the spectra from measurements seem to contain more energy for $f > 5 \cdot 10^{-4}$ Hz, probably related to the energy transfer from smaller scale eddies through strong convection within storms, a theory proposed by [41]. However, it is still a topic of debate on how the energy from small scale turbulence (here shorter than 10 min time scales) is transferred to the larger scales.

For each model grid point, the 50-year winds were calculated for 10 m, 15 m, 52 m and 105 m, with 10 m the diagnostic level and the other three as the lowest three model levels. Figure 7a and 8a are examples of the 50-year wind atlases at 10 m for Denmark and the Gulf of Suez. The 50-year wind values at 15 m, 52 m and 105 m were interpolated to obtain the 50-year wind at the corresponding measurement height by using a second-order polynomial. The results for the grid points closest to the sites are listed in Table III. Using a first order linear interpolation at the two neighboring heights gives similar but slightly smaller values by 0.4 ms^{-1} on average. In this qualitative comparison, the WRF U_{50} values are underestimated compared to the measured ones. It is anticipated that there are larger uncertainties at lower measurement heights where measurements are more influenced by local terrain effect that are not taken into account in the mesoscale modeling.

The atlases of the generalized 50-year winds $U_{50,st}$ are given in Figure 7b and Figure 8b for the two areas. The values of $U_{50,st}$ at grid points closest to the sites are listed in Table III. The overall agreement is improved, compared to Table III, although the uncertainty in offshore and complex topography remains rather high, e.g. Horns Rev, Risø, El Zayt.

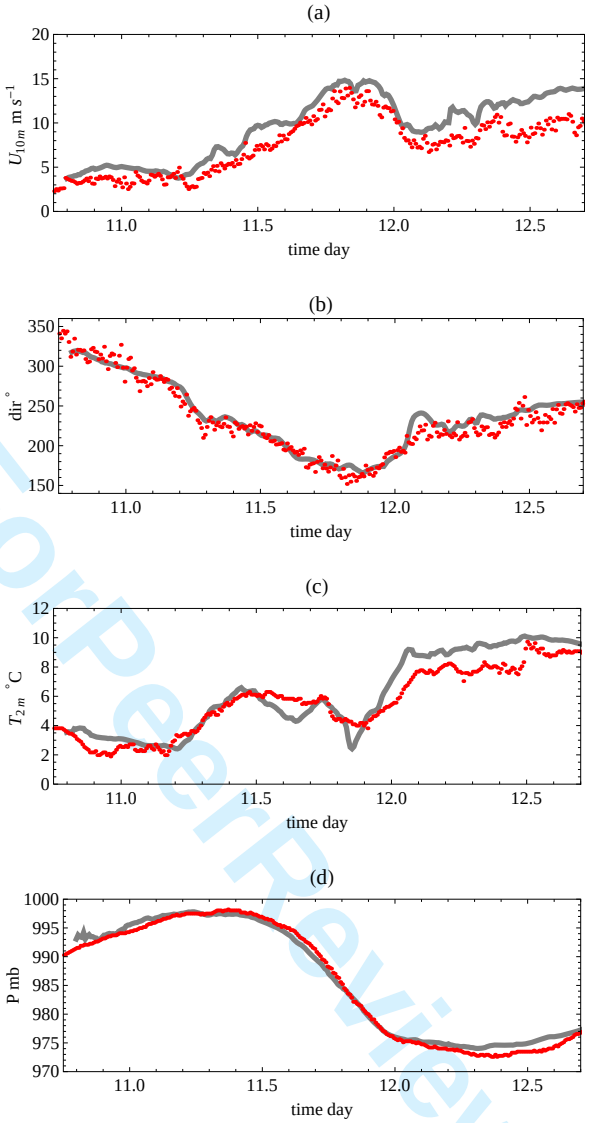

Figure 4. Comparison of measurements (dots) and simulation (thick line) for (a) wind speed at measuring height 10 m, (b) direction, (c) temperature at 2 m and (d) surface pressure at Tystofte during a storm episode from 2010-11-10 18:00 to 2010-11-12 18:00 GMT.

The uncertainties related to each step of the method are discussed in details in the next section.

5. DISCUSSION

The paper describes a method for estimating extreme wind atlases which is shown to be efficient and feasible. The method is based on a chain of procedures where each step can be validated; this ensures the robustness of the method.

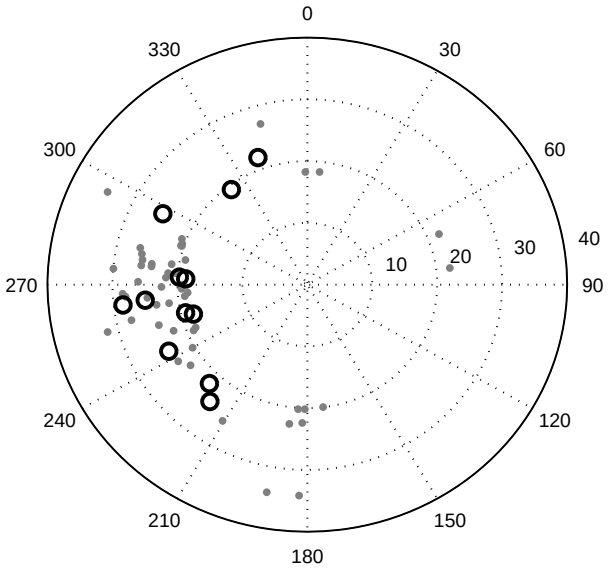

Figure 5. Directional distribution of the measured two strongest winds at 39 m from each year at Tystofte (small gray dots) and that of the WRF simulated annual wind maxima at the same height at the closet grid point to the Tystofte site (black circles). The dashed circles show the wind speed of 0, 10, 20, 30 and 40 ms^{-1}.

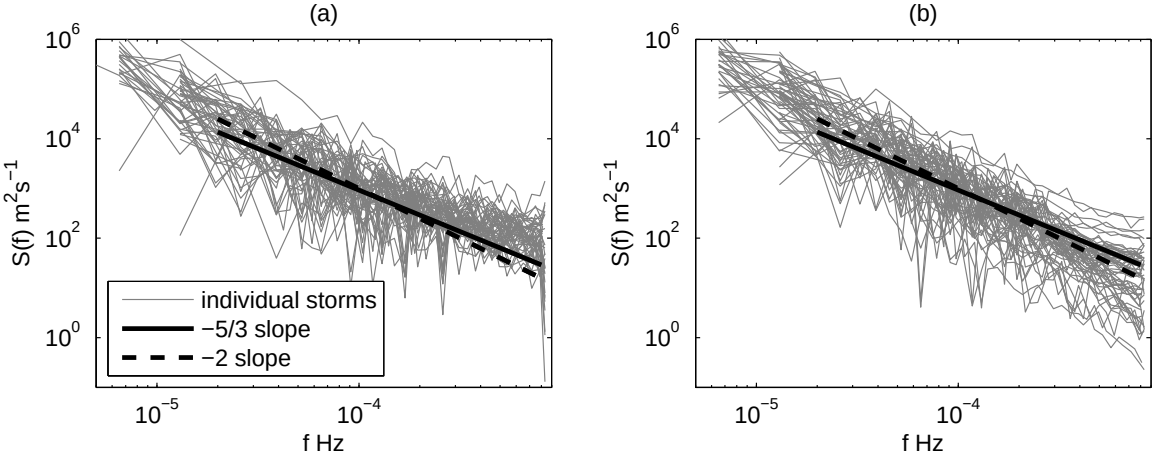

Figure 6. The power spectra of the wind time series from all individual storms at Tystofte 1999-2010 (thin gray) together with a slope of $-5/3$ and a slope of -2, from (a): measurements; (b) closest grid point WRF modeling.

The selective dynamical downscaling method is flexible. If the desired area for the extreme wind atlas needs to be bigger than initially planned, additional storm episodes from additional NRA grid points can simply be added to the existing storm collection. New storms in future years can also be added to the existing collection. The size of the mesoscale model domain can be chosen according to needs although it is recommended to set the outer domain big enough so that the storms can initiate and develop properly. A survey of the storm characteristics regarding the size, general path and life

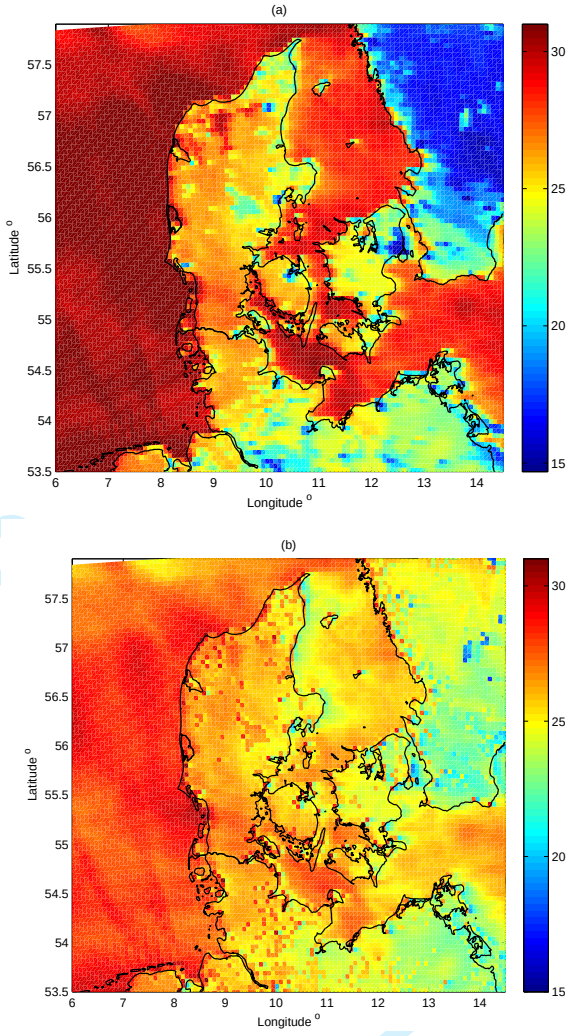

Figure 7. Maps of the 50-year wind over Denmark and surroundings. (a) U_{50} ms^{-1}, the 50-year wind at 10 m calculated with 10 m wind speeds from the WRF model output. (b) $U_{50,st}$ ms^{-1}, the 50-year wind of the standard condition through the post-processing procedure: at 10 m and over homogenous surface with roughness length of 5 cm.

time for a particular area is recommended before the procedure of making the atlas. According to the terrain complexity, the horizontal grid spacing should also be adjusted. Note, the area chosen for storm identification, e.g. Figure 2a and b, does not dictate the mesoscale model domains, it only defines the valid area of the eventual extreme wind atlases. In the post-processing, we have used 12 sectors in the generalization; but it is straightforward to set a different number of sectors depending on the complexity of the local terrain. Based on the distributions of the measured and simulated annual wind maxima at all sites, we used the Annual Maximum Method to obtain the 50-year wind, but other statistical methods, e.g. the Peak-Over-Threshold, can easily be substituted. There are a number of elements within the methodology that could improve its quality. These elements include new global data that are available at higher spatial resolution, which is expected

DOI: 10.1002/we

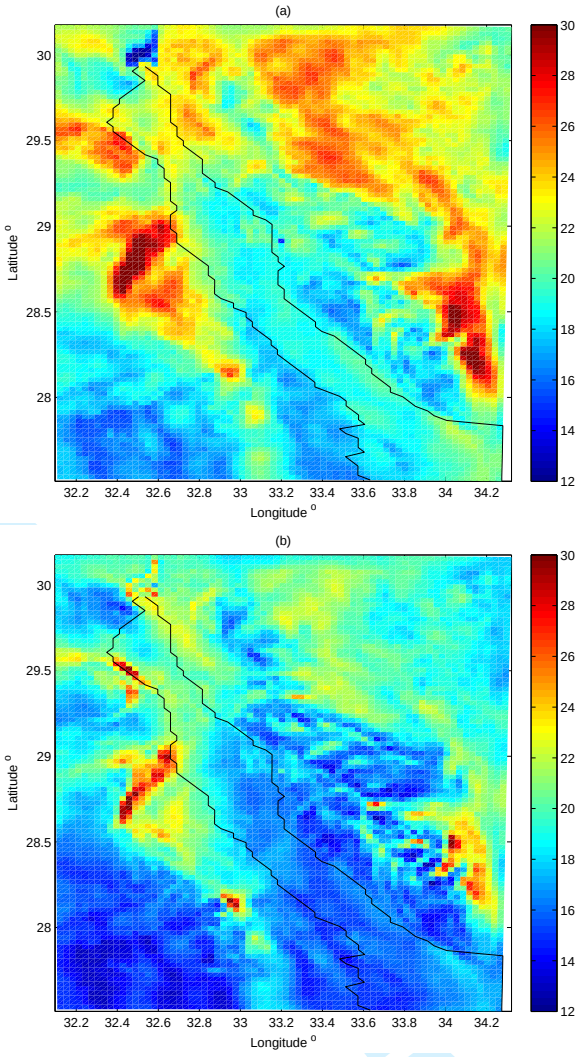

Figure 8. Maps of the 50-year wind over the Gulf of Suez. (a) U_{50} ms^{-1}, the 50-year wind at 10 m calculated with 10 m wind speeds from the WRF modeling. (b) $U_{50,st}$ ms^{-1}, the 50-year wind of the standard condition through the post-processing procedure: at 10 m and over homogenous surface with roughness length of 5 cm.

to serve as better boundary forcing for the mesoscale modeling, e.g. the Climate Forecast System Reanalysis (CFSR) data and ECMWF Interim data. Also, every year there are new parameterizations introduced into the WRF model, even though the actual model core may not have changed. Even for the global final analysis data as used here, more storm samples will be available with as time goes by.

The uncertainty of the method can be attributed to a number of factors. The first is the uncertainty of the WRF simulation in the locations of coastal zone. We chose to use 3 km grid spacing for the inner domain for the Gulf of Suez and 5 km for Denmark. They apparently are able to reproduce the storm evolution accurately, although the uncertainties are considerable in grid boxes that are treated as land but in reality are a mix of water and land (e.g. El Zayt, Risø). As given in Table III, at

JohnWiley&Sons DOI: 10.1002/we

Prepared using weauth.cls

Table III. The 50-year wind at measuring height, $U_{50} \pm 1.96\sigma$, and the 50-year standard wind, i.e. at 10 m, over roughness of 0.05 m, $U_{50,st} \pm 1.96\sigma$, observed and simulated, and their difference $\Delta U_{50} = U_{50}$(WRF)-U_{50}(OBS), for Denmark (A) and Gulf of Suez (B) cases.
*: values from [9].
x: Corresponding values one and two grid points away from the coast are 20.8 and 21.2 ms $^{-1}$.
+: The corresponding values one and two grid points away from the coast are 16.3 and 17.1 ms $^{-1}$.

		U_{50} ms^{-1}, no generalization				$U_{50,st}$ ms^{-1}, with generalization		
	Stations	Height (m)	WRF	OBS	ΔU_{50}	WRF	OBS	$\Delta U_{50,st}$
A	Sprogø	70	34.2 $\pm$ 6.7	33.0 $\pm$ 3.7	1.2	24.2$\pm$4.4	23.9$\pm$2.0 *	0.3
	Tystofte	39	31.2 $\pm$ 6.6	31.5 $\pm$ 4.5	-0.3	25.0$\pm$5.4	25.7$\pm$2.9 *	-0.7
	Kegnæs	23.4	31.2 $\pm$ 7.0	35.8 $\pm$ 7.0	-4.6	25.8$\pm$5.5	26.3$\pm$3.8 *	-0.5
	Jylex	24	31.8 $\pm$ 6.4	35.4 $\pm$ 5.5	-3.6	27.4$\pm$5.4	29.1$\pm$2.9 *	-1.7
	Risø	76.6	32.0 $\pm$ 6.3	33.2 $\pm$ 5.4	-1.2	25.6$\pm$5.3	23.7 $\pm$ 4.7	1.9
	Høvsøre	100	39.5 $\pm$ 8.0	44.6 $\pm$ 12.5	-5.1	29.7$\pm$5.8	29.8 $\pm$ 9.4	-0.1
	Horns Rev	62	39.3 $\pm$ 7.7	44.2 $\pm$ 14.0	-4.9	29.0$\pm$5.3	31.6$\pm$8.5	-2.6
	FINO1	50	36.5 $\pm$ 6.0	38.1 $\pm$ 8.8	-1.6	27.8$\pm$4.3	27.4$\pm$7.6	0.4
B	Abu Darag	24.5	25.7 $\pm$ 5.8	26.6 $\pm$ 4.0	-0.9	20.5$\pm$4.8	20.2$\pm$3.4	0.3
	Zafarana	24.5	25.4 $\pm$ 5.3	28.1 $\pm$ 4.4	-2.7	19.9$\pm$4.1	19.8 $\pm$ 2.8	0.1
	El Zayt	24.5	20.0 $\pm$ 2.2 (x)	24.5 $\pm$ 3.4	-4.5	15.5$\pm$1.9(+)	17.4$\pm$2.6	-1.9

Risø, $U_{50,st}$ from the simulations is 25.6 ms^{-1} and 23.7 ms^{-1} from the measurements, but the agreement is better before the post-processing. The overestimation of the modeled value after post-processing could be induced by the combined effect of two factors: the diffusive model WRF is not as sensitive to the roughness change as LINCOM, and a roughness length used in WRF is much greater than in reality. The 5×5 km^2 grid box where the Risø station is contained is classified as land in WRF with a roughness length of 5 cm. In reality, the area of this grid box contains a considerable amount of water surface and the actual average roughness length is much smaller than 5 cm. Thus, when correcting the wind to the standard condition of a homogeneous surface with roughness length of 5 cm, the post-processing brings a rather small change to the simulated winds. While for the post-processing of the measured winds, WEng uses much finer resolution orography and roughness data that are much closer to reality, therefore the winds are significantly reduced when being transformed from a small roughness length to the standard condition with a roughness length of 5 cm. Shifting one WRF grid point towards land, the corresponding value becomes 22.0 ms^{-1}, closer to $U_{50,st}$ from measurement. The situation is similar at the Gulf site El Zayt where the topography is complex; by moving one and two grid boxes away from the coast, the values become much closer to the measurements. This simplified analysis shows that the post-processing procedure is not perfect in coastal areas and it is expected that modeling with finer resolution could improve the results. It is also recommended for the time being to consider the analysis of surrounding grid points for the coastline grid points and to make sure both the simulated and the measured values have the same type of surface, i.e. land or water.

The second factor is the fact that the variations in water roughness length are not properly simulated; the Charnock formulation with a coefficient 0.018, as used in WRF, does not properly represent the coastal roughness length during storm conditions. In the current study, we manually enhanced the roughness length using a coefficient of 0.05 based on

DOI: 10.1002/we

measurements from an offshore site, Horns Rev, in order to obtain a smoothing transition of the generalized extreme winds across the coastline. There are still considerable uncertainties in doing so because we have treated the open sea and coastal waters in the same manner. This situation can only be handled properly with a coupled atmospheric and wave dynamics system.

The third factor is the fact that we have used measurements from different periods and lengths. The 50-year winds in Table III have been calculated with the longest record possible. Thus, when comparing the measurements with the simulated extreme wind from 1999 to 2010, we have assumed that the extreme wind climates are the same as represented by the different periods of different lengths. To determine the validity of this assumption, two tests are done. In the first, we calculate U_{50} and $U_{50,st}$ using measured and simulated data from their overlapping period, given that the period is not shorter than 7 years. This calculation can thus be done for Tystofte, Kegnæs, Risø, Høvsøre, Horns Rev and FINO1, with the overlapping period 12, 7, 11, 7, 7, and 7 years, respectively. For the six sites, in order, the corresponding $U_{50,st}$ for the columns of WRF and OBS in Table III, given as (WRF, OBS), are (25.0, 26.8), (27.6, 29.6), (24.8, 24.3), (26.9, 29.8), (32.1, 31.6) and (27.3, 27.4) ms^{-1}, respectively. The overlapping WRF and OBS results are still comparable and the differences are well below the uncertainties of the fitting. Using a record of 7 years gives significantly higher uncertainty from the Gumbel fitting than using a record of 12 years (Eq. (4)); for the measurements used here, the uncertainty due to cutting the time series to the overlapping period can double. For instance, for Kegnæs, $U_{50,st} = 29.6 \pm 5.7$ ms^{-1} obtained from the 7-year data (1999 - 2006) differs considerably from 27.6 $\pm$3.8 ms^{-1} obtained from the 16-year record, even though the difference is within the 95% confidence interval. Because of this we did not add the 50-year winds from the short time series to Table III. In the second test, we investigated the representativity of the extreme wind climate from different periods of different lengths; the longest measured time series from Tystofte, spanning from 1982 to 2009, is used. In Figure 9a, the annual wind maxima at 39 m from the Tystofte mast are plotted. There is barely any visible trend except for the last three numbers. Using the entire time series of 28 years gives a 50-year wind at 39 m of 31.5 ± 4.5 ms^{-1} (Table III). In light of the availability of the 12-year modeled storm data used in our method, the 50-year winds at 39 m are calculated also with this length, running from 1982 and onwards. The results are plotted in Figure 9b as the thin curve for the sixteen 12-year time series. There is some deviation of the values from that using 28-year data but it is well below the uncertainty. The deviation is reduced when using 16-year data (Figure 9c), but it is still very close to using 12-year data. Periods shorter than 12 years were not considered. When we estimate the 50-year wind from the existing data, we also assumed that the extreme wind climate will not change compared to the wind climate for the time period used. The extreme wind climate in the future is yet an unknown factor and beyond the scope of this study.

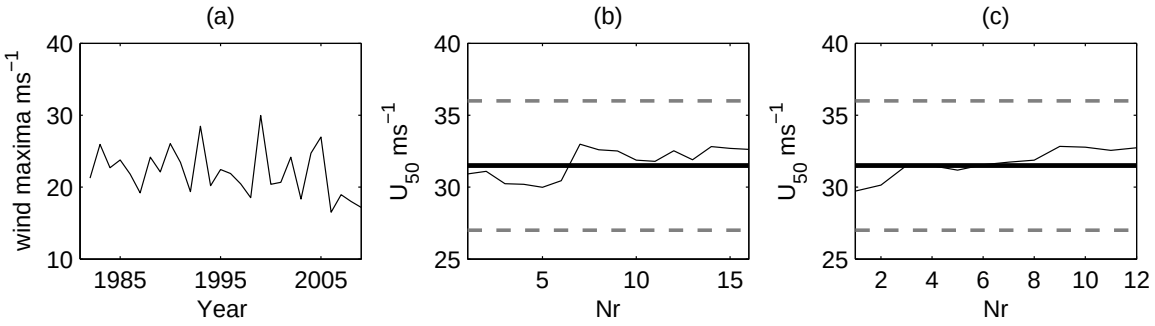

Figure 9. (a) Annual wind maxima at 39 m at Tystofte from 1982 to 2009, 28 years in total. (b) The 50-year wind at 39 m using each 12-year time series running from 1982, for 1982 - 1993, 1983 - 1994, ...1998 - 2009, respectively, 16 values (Nr=16) in total. (c) The 50-year wind at 39 m using each 16-year time series running from 1982, for 1982 - 1997, 1983 - 1998, ..., 1994 - 2009, 12 numbers (Nr=12) in total. U_{50} from 28 years' data, 31.5 ms^{-1}, is drawn in (b) and (c) as the thick line, with the dashed lines showing the 95% confidence interval ± 4.5 ms^{-1} for the Gumbel fitting.

Currently, the validation was made by converting both measured and simulated winds to the same conditions, namely the standard conditions. This, of course, can also be done by converting the simulated winds to the standard conditions and further to the site conditions through microscale modeling, and comparing with the point measurements at the corresponding height. However, this method would not give site-independent validation statistics.

The generalization for measured winds has been done through LINCOM in the software WEng; the generalization for modeled winds has been done using the LINCOM code directly in order to efficiently obtain the correction factors for all grid points. Some differences in the implementation and the roughness corrections for the measurements and mesoscale outputs can cause a bias and we expect improvement in unifying the post-processing procedure in the future.

Note, even though we used the hurricane option in the physics setup, the winds in the two areas studied here were not observed to reach the strength classified as hurricane. For the hurricane impacted areas, the method developed here can be used as well, except that a mesoscale model configuration more suitable for hurricane conditions should be used, e.g. the Hurricane WRF mode.

6. CONCLUSIONS

A method has been developed for obtaining extreme wind atlases for large areas. The method three steps, namely the identification of storm events, the mesoscale modeling of the storms and the post-processing procedure, are feasible and flexible. The method has been applied to two areas, one having the passage of synoptic Atlantic depressions as the cause to the extreme winds and the one having mesoscale channeling of winds contributing significantly to the extreme winds. The

DOI: 10.1002/we

method has shown its ability in producing useful extreme wind atlases, as suggested by the comparison with measurements. The success of this method is probably due to the fact that extreme winds are often linked to synoptic scale dynamics, so that they are identified in the global reanalysis data. Further investigations are needed for areas where purely local mechanisms are responsible for the extreme winds (e.g. thunderstorms).

As a key element, the post-processing makes it possible to compare the simulated and measured data on a more reasonable basis compared to the traditional, direct comparison of the simulated and observed winds. In addition, the post-processing makes it possible to import mesoscale modeled results to microscale modeling, (e.g. WEng) to obtain site-specific extreme winds (not demonstrated in this paper).

Higher uncertainties in the extreme wind estimation were observed in complex terrain such as along the coast, which highlights the need for improvement in the mesoscale modeling and the post-processing in these areas. There are also higher uncertainties over water where the surface waves were not dynamically coupled to the atmosphere in the modeling.

ACKNOWLEDGEMENTS This work is supported by the Danish grant 2009-1-10240 “Calculation of Extreme Wind Atlases Using Mesoscale Modelling” and EU SafeWind project (no. 213740). We acknowledge DONG Energy for the measurements from Horns Rev and Nysted, and the EU Norsewind project for the measurements at FINO1. We thank Jakob Mann for comments. The NCEP/NCAR data are provided by the NOAA-CIRES Climate Diagnostics Centre, Boulder, Colorado, from their web site at http://www.cdc.noaa.gov/. The FNL data are from the Research Data Archive (RDA) which is maintained by the Computational and Information Systems Laboratory (CISL) at NCAR.

REFERENCES

1. Eurocode. Eurocode 1, Basis of design and actions on structure – Parts 2 – 4: Actions on structure – Wind actions. *Technical Report*, European Committee for Standardization, Rue de Stassart, Brussels 1995.
2. Gumbel EJ. *Statistics of Extremes*. Columbia University Press, 1958.
3. Coles S. *An Introduction to Statistical Modeling of Extreme Values*. Springer-Verlag, London, UK, 2001.
4. Mann J, Kristensen L, Jensen NO. Uncertainties of extreme winds, spectra and coherences. *Bridge Aerodynamics, ISBN 9054109610*, Larsen, Esdahl (eds.). Rotterdam: Balkema, 1998.
5. Gross J, Heckert A, Lechner J, Simiu E. Novel extreme value estimation procedures: Application to extreme wind data. *Extreme Value Theory and Applications*, Galambos J, Lechner J, Simiu E (eds.). Kluwer, Boston, 1994.

6. Palutikof JP, Brabson BB, Lister DH, Adcock ST. A review of methods to calculate extreme wind speeds. *Meteorological Applications* 1999; **6**:119–132.
7. Kalnay E, Kanamitsu M, Kistler R, Collins W, Deaven D, Gandin L, Iredell M, Saha S, White G, Woollen J, *et al.*. The NCEP/NCAR 40-year reanalysis project. *Bull. Am. Meteorol. Soc.* 1996; **77**:437–471.
8. Frank H. Extreme winds over Denmark from the NCEP/NCAR reanalysis. *Technical Report Risoe-R-1238(EN)*, Risø National Laboratory, Roskilde, Denmark, *http://www.risoe.dk/rispubl/VEA/ris-r-1238.htm* 2001.
9. Larsén XG, Mann J. Extreme winds from the NCEP/NCAR reanalysis data. *Wind Energy* 2009; **12**:556–573, doi: 10.1002/we.318.
10. Tennekes H. Similarity relations, scaling laws and spectral dynamics. *Atmospheric Turbulence and Air Pollution Modelling*, Nieuwstadt FTM, van Dop H (eds.). chap. 2, D. Reidel Publishing Company: Dordrecht, 1982; 37–68.
11. Larsén XG, Mann J, Berg J, Göttel H, Jacob D. Wind climate from the regional climate model REMO. *Wind Energy* 2010; **13**:279–296, doi:10.1002/we.337.
12. Badger J, Larsén XG, Mortensen N, Hahmann AN, Hensen J, Jørgensen H. A universal mesoscale to microscale modelling interface tool. European Wind Energy Conference, Warsaw, Poland, 20 - 23 April, 6 pages, 2010.
13. Davenport A. The relationship of wind structure to wind loading. *Wind Effects on Buildings and Structures, Proceedings of the first conference on wind effects on buildings and structures*. HMSO: London, 1963; 53–102.
14. Kristensen L, Rathmann O, Hansen SO. Extreme winds in Denmark. *J. Wind Eng. Ind. Aerodyn.* 2000; **87**:147–166.
15. Miller C. A once in 50-year wind speed map for Europe derived from mean sea level pressure measurements. *J. Wind Eng. Ind. Aerodyn.* 2003; **91**:1813–1826.
16. Weisse R, Storch H, Feser F. Northeast Atlantic and North Sea storminess as simulated by a regional climate model during 1958-2001 and comparisons with observations. *Journal of Climate* 2005; **18**:465–479.
17. Winterfeldt J. Comparison of measured and simulated wind speed data in the North Atlantic. *Technical Report PhD-Thesis, ISBN 0344-9629*, GKSS-Forschungszentrum Geesthacht GmbH, GKSS Library, Postfach 11 60, D-21494 Geesthacht, Germany 2008.
18. Nielsen NW, Sass BH. A numerical, high resolution study of the life cycle of the severe storm over Denmark on 3 December 1999. *Tellus* 2003; **55**:338–351.
19. Larsén XG, Ott S, Badger J, Hahmann AH, Mann J. Recipes for correcting the impact of effective mesoscale resolution on the estimation of extreme winds. *J. Appl. Meteorol. Climat.* 2012; **51**(3):521–533, doi:10.1175/JAMC-D-11-090.1.

20. Larsén XG, Mann J, Göttel H, Jacob D. Wind climate and extreme winds from the regional climate model REMO. In: Scientific Proceedings (on line). European Wind Energy Conference and Exhibition, Brussels, 31 March - 3 April, 2008; 58–62.
21. Pryor SC, Barthelmie RJ, Clausen NE, Drews M, Mackeller N, Kjellström E. Analysis of possible changes in intense and extreme wind speeds over northern Europe under climate change scenarios. *Clim. Dyn.* 2010; doi: 10.1007/s00382-010-0955-3.
22. Hofherr T, Kunz M. Extreme wind climatology of winter storms in Germany. *Clim. Res.* 2010; **41**:105–123.
23. Kunz M, Mohr S, Rauthe M, Lux R, Kottmeier C. Assessment of extreme wind speeds from regional climate models - Part 1: Estimation of return values and their evaluation. *Nat. Hazards Earth Syst. Sci.* 2010; **10**:907–922.
24. Mortensen NG, Hansen JC, Badger J, Jørgensen BH, Hasager CB, Youssef LG, Said U, Moussa A, Mahmoud M, Yousef A, *et al.*. *Wind atlas for Egypt, Measurements and Modelling 1991 - 2005*. Risø National Laboratory, New and renewable energy authority, Cairo, Egypt and Egyptian meteorological authority, ISBN 87-550-3493-4, 2005.
25. Holmes J, Moriarty W. Application of the generalized pareto distribution to extreme value analysis in wind engineering. *J. Wind Eng. Ind. Aerodyn.* 1999; **83**:1–10.
26. Abild J. Application of the wind atlas method to extremes of wind climatology. *Technical Report Risoe-R-722(EN)*, Risø National Laboratory, Roskilde, Denmark 1994.
27. Hosking J. Estimation of the generalized extreme value distribution by the method of probability-weighted moments. *Technometrics* 1985; **27**:251–261.
28. Kwun JH, Kim Y, Seo J, Jeong J, You SH. Sensitivity of MM5 and WRF mesoscale model prediction of surface winds in a typhoon to planetary boundary layer parameterization. *Nat Hazards* 2009; **51**:63–77.
29. Draxl C, Hahmann AH, Peña A, Giebel G. Evaluating winds and vertical wind shear from WRF model forecasting using seven PBL schemes. *Wind Energy, conditionally accepted.* 2012; .
30. Skamarock W, Klemp J, Dudhia J, Gill D, Barker D, Wang W, Powers J. A Description of Advanced Research WRF. *Technical Report NCAR/TN-468+STR*, NCAR, NCAR, Boulder, Colorado, USA 2007.
31. Gilleland E, Ahijevych DA, Brown BG, Casati B, Ebert EE. Intercomparison of spatially forecast verification methods. *Wea. Forecasting* 2009; **24**:1416–1430, doi:10.1175/2009WAF2222269.1.
32. Gilleland E, Ahijevych DA, Brown BG, Ebert EE. Verifying forecasts spatially. *BAMS* 2010; :1365–1373doi: 10.1175/2010BAMS2819.1.

33. Yates E, Anquetin S, Ducrocq V, Creutin JD, Ricard D, Chancibault K. Point and areal validation of forecast precipitation fields. *Meteorol. Appl.* 2006; **13**:1–20.

34. Mann J, Larsén XG, Jørgensen HE. Regional extreme wind climates and local winds. The one day conference on extreme winds and developments in modelling of wind storms, Cranfield University, 15th Sep., (17), *http://www.waspengineering.dk/ExtremeAtlas/RMS4pageAbstract.pdf*, 2004.

35. Astrup P, Jensen NO, Mikkelsen T. Surface roughness model for LINCOM. *Technical Report Risø-R-900*, Risø National Laboratory, Roskilde, Denmark, *URL:www.risoe.dk* 1996.

36. Astrup P, Larsen SE. WAsP Engineering flow model for wind wind over land and sea. *Technical Report Risø-R-1107*, Risø National Laboratory, Roskilde, Denmark, *URL:www.risoe.dk* 1999.

37. Landberg L, Myllerup L, Rathmann O, Petersen EL, Jørgensen BH, Badger J, Mortensen N. Wind resource estimation – An overview. *Wind Energy* 2003; **6**:261–271.

38. Charnock H. Wind stress on a water surface. *Q. J. R. Meteorol. Soc.* 1955; **81**:639–640.

39. Skamarock W. Evaluating mesoscale NWP models using kinetic energy spectra. *Monthly Weather Review* 2004; **132**:3019–3032.

40. Larsén XG, Vincent CL, Larsen S. Spectral structure of the mesoscale winds over the water. *Q. J. R. Meteorol. Soc., In press* 2012; .

41. Lilly D. Stratified turbulence and the mesoscale variability of the atmosphere. *J. Atmos. Sci* 1983; **40**:749–761.